A Regime Shift in the Interhemispheric Teleconnection between the Yellow and East China Seas and The Southeastern Tropical Pacific in The Southern Hemisphere during The Boreal Summer

Yong Sun Kim
Korea Institute of Ocean Science and Technology
Minho Kwon
Korea Institute of Ocean Science and Technology
Eui-Seok Chung
Korea Polar Research Institute
Sang-Wook Yeh
Hanyang University
Jin-Yong Jeong
Korea Institute of Ocean Science and Technology
Chan Joo Jang (cjjang@kiost.ac.kr)
Korea Institute of Ocean Science and Technology https://orcid.org/0000-0001-9475-9429

Research Article

Keywords: El Niño-Southern Oscillation (ENSO), Yellow and East China Seas, Regime Shift, East Asian Summer Monsoon, South Pacific Meridional Mode (SPMM)

Posted Date: October 22nd, 2021

DOI: https://doi.org/10.21203/rs.3.rs-949462/v1

A regime shift in the interhemispheric teleconnection between the Yellow and East China Seas and the southeastern tropical Pacific in the Southern Hemisphere during the boreal summer

Yong Sun Kim[1, 2], Minho Kwon[1, 2], Eui-Seok Chung[3], Sang-Wook Yeh[4], Jin-Yong Jeong[5], and Chan Joo Jang[1, 6*]

[1]Ocean Circulation Research Center, Korea Institute of Ocean Science and Technology, Busan, Korea

[2]Ocean Science and Technology School, Korea Maritime and Ocean University, Busan, Korea

[3]Divison of Atmospheric Sciences, Korea Polar Research Institute, Incheon, Korea

[4]Department of Marine Sciences and Convergent Technology, Hanyang University, ERICA, Ansan, Korea

[5]Marine Disaster Research Center, Institute of Ocean Science and Technology, Busan, Korea

[6]Department of Integrated Ocean Sciences, University of Science and Technology, Daejeon, Korea

For Climate Dynamics

September 2021

[*]Corresponding Author:

Korea Institute of Ocean Science and Technology, 385 Haeyangro, Yeong-do, Busan, Republic of Korea, 49111 e-mail: cjjang@kiost.ac.kr

Abstract

[1] Through statistical estimations on reconstructed datasets for the period 1982−2020 after removing a long-term trend, we observed that there was a drastic regime shift in the early summer's connection between the YECS and the tropical Pacific in the early 2000s. The summer YECS SSTs had seemed to be modulated by local oceanic and atmospheric processes along with their marginal coupling to the tropical Pacific during the pre-2003 period before the regime shift. In contrast, an interhemispheric YECS−tropical southeastern Pacific (SEP) coupling appeared after the regime shift. This teleconnection was at least partially attributed to a reduced El Niño signature in the tropical Pacific, which favors the emergence of the South Pacific meridional mode (SPMM) independently from ENSO signals. Precipitation anomalies in the western tropical Pacific act as an atmospheric bridge to mediate the air-sea interacted variability associated with the SPMM into the North Pacific. The susceptibility of the YECS to atmospheric forcing may highlight the role of SST over the YECS as a potential indicator of basin-scale climate changes.

Keywords: El Niño-Southern Oscillation (ENSO), Yellow and East China Seas, Regime Shift, East Asian Summer Monsoon, South Pacific Meridional Mode (SPMM)

1. Introduction

[2] The Yellow and the East China Seas (hereafter YECS; Figure 1a) comprise a well-developed continental shelf supporting productive values as a vast marine ecosystem in the northwestern Pacific marginal seas (e.g., Beardsley et al. 1985; Fan and Huang 2008; Belkin 2009), and have undergone substantial long-term changes in their physical and ecological environments over the last few decades (Belkin 2009; Yeh and Kim 2010; Bao and Ren 2014; Liao et al. 2015; Park et al. 2015; Cai et al. 2017). Research into climate change in the YECS has been focused on the winter sea surface temperature (SST), which represents a primary mode of long-term variability along with the recognition of a remarkable linear trend during the last few decades (Yeh and Kim 2010; Zhang et al. 2010; Bao and Ren 2014; Cai et al. 2017; Kim et al. 2018). Less is known about a mechanism for summer SST interannual variability, even though a variance several times greater was estimated relative to that for the winter SST in the YECS (Supplementary Figure S1a).

[3] A key process which has been known to regulate local winds, precipitation, typhoons, and thereby to determine the amplitude of the East Asian summer monsoon (EASM; Ha et al. 2012; Seok and Seo 2021), might be associated with the western North Pacific Subtropical High (wNPSH; e.g., Wang et al. 2000, 2013; Yang and Lau 2004; Yim et al. 2008; Du et al. 2011; Fan et al. 2013; Liu et al. 2013; Xiang et al. 2013; Xie et al. 2016). The anomalous wNPSH is triggered by a cold sea surface anomaly, presumably after equatorial Pacific warming (i.e., El Niño) reaches its mature phases during the boreal winter months (Wang et al. 2000, 2013; Yang and Lau 2004; Xie et al. 2016). Therefore, the literature has postulated a causal relationship between El Niño and YECS summer SST with a lag of several months (e.g., Wang et al. 2000; Park and Oh 2000; Liu et al. 2013; Wu et al. 2016). Reported correlations are, however, generally low, along with an

inconsistent forcing region between studies. Wu et al. (2016), for instance, demonstrated that SST anomalies after removing long-term trends and annual cycles in the YECS (24−42°N/117−130°E) rendered a correlation of 0.31 over six months preceding the Nino3 SST index (SST anomaly averaged over 5°S−5°N/150°W−90°W) for the period 1982−2011. Liu et al. (2013) demonstrated that the China Seas warmed for around 4–10 months after the equatorial Pacific SST anomalies reached their maximum. A power spectrum coherency analysis also showed that anomalous SSTs in the East Asian marginal seas (25−45°N/117−141°E) varied coherently for 5−9 months preceding the Nino34 (5°S−5°N/170°W−120°W) SST index, particularly on a 2−3-year frequency band during the period 1951−1996 (Park and Oh 2000). Meanwhile, several studies pointed out the importance of cooling anomalies in the central equatorial Pacific, i.e., the Nino4 region (5°S−5°N, 160°E−150°W), in strengthening the wNPSH, especially during the development phase of La Niña (Lau and Nath 1996; Fan et al. 2013; Wang et al. 2013), thus suggesting an asymmetric response of summer SST anomalies to El Niño and La Niña events (Hardiman et al. 2018).

[4] The discrepancy in the literature on the relationship between the summer SST anomaly of the YECS and ENSO forcing regions could be reconciled with the consideration of an El Niño flavor and the existence of ENSO precursors. First, the flavor is believed to have changed between two types – the canonical eastern Pacific warming type El Niño (EP El Niño) and the central Pacific warming type El Niño (CP El Niño). The latter is known to have occurred more frequently than the typical EP El Niño in recent decades (e.g., Yeh et al. 2009; Di Lorenzo et al. 2010; Yeo et al. 2012; Xiang et al. 2013; Jo et al. 2015; Capotondi et al. 2015; Yeh et al. 2015; Stuecker 2018) due to global warming (Yeh et al., 2009; Yeo and Kim 2014), and its positive feedback with the North Pacific meridional mode and thus enhanced coupling between the CP El Niño and meridional

mode (Liguori and Di Lorenzo, 2018; Stuecker, 2018). A shift in the flavor would trigger resultant interactions between SST and atmospheric variables such as wind, heat flux, and precipitation in the forcing region, possibly yielding a marginal teleconnection between the YECS and equatorial Pacific if studies do not consider the abrupt change of a forcing region. The second candidate that accounts for this discrepancy is the existence of ENSO precursors: North/South Pacific meridional modes (e.g., Vimont et al. 2003; Chang et al. 2007; Zhang et al. 2014a; Min et al. 2017; You and Furtado 2017; Larson et al. 2018; Stuecker 2018; Zhang et al. 2021). Approximately two or three seasons before an El Niño event reaches its mature phase, a weakening of the off-equatorial trade winds modulates latent heat fluxes, thereby exciting warm SST anomalies along the western coasts of North/South America (Vimont et al. 2003; Chang et al. 2007; Zhang et al. 2014a). These temperature anomalies tend to extend toward the equatorial Pacific via the Wind-Evaporation-SST (WES) feedback and background current, modulate precipitation over the Inter-Tropical Convergence Zone (ITCZ), and thus form an extratropical teleconnection by altering the Rossby wave train (Trenberth et al. 1998; Deser and Phillips 2004; He et al. 2011; Wu et al. 2015). If these meridional modes directly impact the summer monsoon in the western North Pacific, the low correlations estimated from the YECS summer SST and the ENSO SST indices in previous studies might be justifiable.

[5] This study aims to investigate the teleconnected impact of the tropical Pacific on the YECS summer SSTs by considering these two hypotheses. To elucidate the atmospheric bridge connecting the equatorial Pacific and the YECS, we have characterized the large-scale atmospheric circulation and precipitation anomalies associated with the year-to-year summer SST variance in the YECS. Here, we will contrast the large-scale atmospheric and oceanic fields in shaping the

summer SSTs in the YECS; the EP El Niño-like pattern seems to have played a role in modulating the EASM through forming wind anomalies by the wNPSH, but to have left a marginal signal in the YECS summer SSTs before the early 2000s, while the South Pacific Meridional Mode (SPMM hereafter; Zhang et al. 2014a) has determined the YECS summer SSTs likely through modulating the Rossby wave train initiated from the western Pacific precipitation anomaly in recent summers when the EP El Niño was inactive after the early 2000s.

[6] The rest of this paper is structured as follows. Section 2 describes the observational and reanalysis datasets and analysis methods. Section 3 shows that the regime shift in terms of teleconnection between these two regions took place in the early 2000s. In section 4, we discuss that this regime shift could be related to the mean state of the equatorial Pacific. Section 5 contains the summary and conclusions.

2. Data and methods

[7] This study has analyzed mainly OISSTv2 data from the National Oceanic and Atmospheric Administration (NOAA; Reynolds et al. 2007) for the recent 39-year period of 1982−2020 with the spatial resolution of 1/4°×1/4°. This dataset is optimally merged based on Advanced Very High-Resolution Radiometer (AVHRR) observations with ancillary in-situ measurements. Inter-comparison studies have suggested that the OISSTv2 is consistent with surface drifters and other SST datasets, not only in open oceans (Reynolds and Chelton 2010) but also in coastal seas (Lima and Wethey 2012; Liao et al. 2015; see Figure S1) with the unique advantage of a persistent quality over almost four decades. Considering the spatial coverage of the YECS (117−129.5°E/26−41°N) spanning 12.5° longitude by 15° latitude, the OISSTv2 might be a unique and pertinent dataset for

this long-term SST variability study in the YECS. Other reanalysis datasets with coarser resolutions such as the Hadley Centre Ice and Sea Surface Temperature (HadISST; 1° horizontal resolution; Rayner et al. 2003) or the Extended Reconstructed Sea Surface Temperature (ERSSTv5; 2° resolution) do not alter our results, as discussed below in section 3.1. The domain does not fully cover the southern part of the East China Sea in order to exclude a local impact from the Kuroshio Current; our findings presented here are not sensitive to the meridional span of the domain (not shown). In this study, spring and summer both refer to the boreal seasons.

[8] We estimated monthly anomalies by subtracting the study period (1982−2020) means from each calendar month and a linear trend at each grid point. The average SST trend throughout the YECS was 0.22°C per decade, which accounts for 26.5% of the total variance after the seasonal cycle was removed. The early summer of May−June−July (hereafter MJJ) means were computed from the monthly anomalies to disengage a sub-seasonal perturbation associated with a tropical cyclone. The genesis of the tropical cyclone and its activity over the western North Pacific form a climatological peak in August and September as the cross-equatorial flows and monsoonal westerlies fully develop (Wang and Zhou 2008; Choi and Ha 2018), thereby tending to leave impulsive signals on the climatic variability of summer SSTs over the YECS (Park et al. 2019).

[9] This study has employed primary statistical tools, including linear regression, correlation, and the singular value decomposition (SVD, also known as maximum covariance analysis) analyses, to identify an atmospheric pattern that evolves coherently with the MJJ mean SST of the YECS. We define the MJJ SST anomalies averaged over the YECS as a YECS summer SST index (Figure 1b). This index is almost identical to the primary PC time series (PC1) for the summer SST anomalies in the YECS with a correlation coefficient of 0.90 between this index and the PC1,

which explains approximately 51% of the total year-to-year SST variance of the YECS, and is clearly separate from higher modes according to North et al. (1982). To identify an atmospheric bridge, we have analyzed the Climate Prediction Center (CPC) Merged Analysis of Precipitation (CMAP) data (Xie and Arkin 1997), as well as wind, geopotential height, precipitation fields from the fifth-generation European Centre for Medium-range Weather Forecasts (ECMWF) atmospheric reanalysis for the period 1982−2020 with a spatial resolution of 0.5° (Hersbach et al. 2020). For the statistical significance test, we estimated a p-value based on a two-tailed student's t-test with an effective degree of freedom computed considering a lag-1 autocorrelation in the time series (Bretherton et al. 1999).

3. Results

3.1 *Relationship of the YECS summer SST with Pacific and Indian Ocean SSTs*

[10] Figure 2a shows the simultaneous correlation map of the SST anomalies in the Pacific and Indian Oceans to the YECS SST index for 39 years (1982−2020). The coefficients that are statistically significant at a 90% confidence level are displayed in Figure 2a. Apparent correlations appear in three regions: the mid-latitude of the Northwest Pacific around the YECS, the southeast tropical Pacific (SEP; 20−10°S/130°−100°W, red box) near South America, and the southwest tropical Indian near the east of Madagascar Island (hereafter SWI; 25−17°S/35−60°E). While high correlations around the YECS seem reasonable, those in the Southern Hemisphere are unexpected. The correlations, however, are barely significant at a 95% confidence level for the SEP ($r = 0.42$) and at a 90% confidence level for the SWI ($r = -0.34$). We plot the time series of the YECS and the SEP averaged SST anomalies together in Figure 2b, which represents a contrast in the SST

temporal evolution of the YECS and SEP regions before and after the early 2000s: the year-to-year fluctuation of the summer YECS SST anomalies (the black bars in Figure 2b) was precisely in tune with those of the SEP (the red line) only during the later years of the period 2003−2020 (r = 0.74), but not during the early years of the period 1982−2002 (r = 0.19). A similar contrast with a reduced correlation for the later years was estimated for the SWI (not shown).

[11] The correlations between the YECS summer SST index and the SEP SST anomalies that were estimated by applying a nine-year sliding window also rendered a robust YECS-SEP coupling only during the period after the 2000s (Figure 2c). An eleven-year window, or a seven-year one, yielded a similar result. The correlation in the sliding estimation went up to 0.94 in around early 2010, and then tended to decrease slightly in the last few years. The sliding correlations that applied to the HadISST, which spanned the period 1900−2020, were similar to those shown in Figure 2c: the significant correlations between the YECS and the SEP/SWI SST anomalies during the recent years after the early 2000s (not shown). The ERSSTv5, which has a further coarse horizontal resolution of 2°, also yielded significant correlation coefficients but only with the SEP SST for the period after the late 1990s. These results suggest the insensitivity of one of our key findings – a regime shift that happened at least throughout the early 2000s in terms of the YECS-SEP summer SST teleconnection – to the dataset. It is noteworthy that the calculated correlations for the pre-satellite era are of questionable quality due to the lack of in-situ observations in both the YECS and SEP/SWI regions (Kim et al. 2018; Zhang et al. 2014a; Zhang et al. 2021).

[12] Since previous articles have suggested a lagged relationship between the equatorial Pacific SSTs and summer SSTs around the YECS, this study conducted a lead-lag cross-correlation analysis between the YECS summer SST index and the SST anomalies for the periods 1982−2002

(Figure 3a-e) and 2003−2020 (Figure 3f-j), respectively, before and after the regime shift with various time lags between four months preceding (i.e., JFM) and four months following (SON) our study months. With regard to the contribution of the equatorial Pacific SSTs to the YECS summer SST variance, we failed to find a meaningful correlation in the eastern or central Pacific for any lagged month for both periods before and after the early 2000s. Insignificant correlations less than ±0.15 between the YECS summer SST index and the lead-lag ENSO indices for different regions − Nino3, Nino3.4, and Nino4 − might be more evidence for the ENSOs' marginal forcing role in altering the summer YECS SSTs (Figure S2). Besides, any significant relationship does not stand between the YECS summer SST index and either the Pacific Decadal Oscillation (PDO) – a low-frequency modulation of the ENSO – or the Atlantic Multidecadal Oscillation (AMO; Figure S2), which has been mentioned in previous articles as a key index for modulating low-frequency SST variability in the YECS (Zhang et al. 2010; Liao et al. 2015; Kim et al. 2018).

[13] During the period before the regime shift, a region characterized by close correlations begins to appear during the JFM months in the South China Sea (Figure 3a), which is geographically connected upstream of the Taiwan warm current to the YECS through the Taiwan Strait. The region of close correlations seems to expand northward toward the South China Sea (Figure 3b), then turns eastward to the East/Japan Sea and the Northwest Pacific, presumably associated with local currents and winds (Figure 3c-3e; Cai et al. 2017; Kim et al. 2018). For years after the regime shift, in contrast, a region of robust correlations in the SEP off the coast of Chile emerged almost four months before the early summer (Figure 3f). The correlations reached a maximum of up to 0.85 at a lag of –2 months (Figure 3g). After that, the region of robust correlations seemed to spread diagonally toward the western Pacific warming pool between the equator and the southern

South Pacific Convergence Zone (SPCZ). Next, we will explore how the SEP affected the year-to-year summer variance of the YECS during each period.

3.2 *Atmospheric fields in association with the summer YECS index*

a. Before the regime shift

[14] This section investigates atmospheric fields in the context of regime shift; the linear fractions of those variables − SST, precipitation, wind (U850), geopotential height (H850) at 850 hPa, and meridional winds along the dateline − that are congruent with the YECS summer SST index (Figure 4); the magnitudes of the regressed fields represent anomalies corresponding to one standard deviation of the YECS SST index. Before the regime shift, positively regressed SST anomalies which extended from the YECS toward the center of the North Pacific aligned with easterly wind anomalies (Figure 4a). These anomalies represented a weakening of the mean westerly winds over the North Pacific, thus decreasing turbulent heat fluxes into the atmosphere and, in turn, likely resulting in oceanic warming (e.g., Yeh and Kim 2010; Cai et al. 2017; Kim et al. 2018). A positive geopotential height anomaly located northeast of the YECS centered at 42°N and 180°E, and a negative one centered around 140°E and 25°N within the western North Pacific seemed to generate these easterly wind anomalies in the mid-latitudes. The negative one (i.e., low-pressure anomaly) was accompanied by southwest-northeast-oriented enhanced rainfall throughout the western subtropical North Pacific and suppressed rainfall over the East China Sea and southern East/Japan Sea (Figure 5b). Another remarkably dry anomaly appeared in the region west of the dateline around the equator that was associated with a lower-level divergence of the

meridional winds and an upper-level convergence around the equator that invoked a descending motion near the equator (Figures 4b; 4c).

[15] This low-pressure anomaly in the western North Pacific that was accompanied by a tripole structure of precipitation anomalies bore a resemblance, but opposite to the primary EOF mode (EOF1) estimated from H850 over the Asian-Australian monsoon domain (20°S−40°N, 30°E−180°E; refer to Figures 2a and 2b in Wang et al. 2013). This pattern represented the southwest-northeast tilted wNPSH. The spatial analogy might hint at the role of the eastern equatorial Pacific and the northern Indian Ocean in shaping the EASM through modulating the tilted wNPSH during the period before the regime shift (Wang et al. 2000, 2013; Yim et al. 2008; Xiang et al. 2013; Xie et al. 2016). However, the teleconnected influence of the eastern equatorial Pacific and Indian Ocean on the YECS SST anomalies seemed statistically insignificant during the early period before the regime shift, as demonstrated in Figures 2 and 3.

b. After the regime shift

[16] The YECS-wNPSH coupling has no longer been pertinent in recent summers after the regime shift (Figure 4d-f). The high SST that had previously extended from the YECS into the central North Pacific (Figure 4a) seems to have been confined within the YECS after the regime shift (Figure 4d). The eastward limit of high temperatures and dry anomalies is likely demarcated by a low-pressure anomaly extending from the northeastern Pacific to the southwest. This SST regression in the YECS appears with a positive geopotential height anomaly of 4 m and a negative precipitation anomaly higher than −1.6 mm/day, implying a clear sky and increased solar radiation for warm summer SSTs in the YECS.

[17] Although the regressions are on the YECS summer SST index, more remarkable atmospheric and oceanic signals have appeared in the Southern Hemisphere in recent years, such as a zonal dipole pattern of high and low geopotential heights from the west to the east over the Indian and the Pacific Oceans (Figure 4e). This large-scale atmospheric circulation field invokes southerly winds from the south over the SWI and southwestern tropical Pacific, resulting in cold SST anomalies, while northerly wind anomalies from the equator in the southeastern tropical Indian and SEP regions (Figure 5d) contribute to warm SST anomalies. This large-scale atmospheric circulation reminds us of the role of air-sea turbulent fluxes in forming a wave-like subtropical dipole in the Southern Hemisphere (Wang 2010; Zhang et al. 2014a). This tropical SST variation, particularly in the SEP, could be enhanced by the WES feedback (Zhang et al. 2014a) and interactive ocean dynamics (Okumura 2013), and seems to contribute to the convective precipitation in the western equatorial Pacific around the dateline (enhanced rainfall) and ITCZ (reduced rainfall) by affecting the meridional winds (Figure 4e and 4f; see section 4.2 for a more detailed discussion).

[18] One of most important features during the recent period might be a “hemispheric symmetry” both in H850 and precipitation over the Pacific Ocean, as shown in Figure 4e. First, there are meridional dipole patterns of positive- and negative-pressure anomalies from high to low latitudes in both hemispheres. The pressure pattern in the Southern Hemisphere is the South Pacific Oscillation (SPO), with a meridional dipole pattern and barotropic structure throughout the troposphere over mid to high latitudes (You and Furtado 2017; Figure 4e, 4f). In addition, a weak high-pressure anomaly over the YECS mirrors one occupying the east of Australia. In the precipitation field, the hemispheric symmetry seems to be centered with a negative precipitation

anomaly on the ITCZ around 7°N, and is associated with the divergence of low-level winds, as shown in Figure 4f. Outside the ITCZ, a band of intensified rainfall has appeared as a tilted feature in the north of the SPCZ, with a weaker one extending toward the center of the North Pacific. On the poleward sides, negative anomalies are located over the SPCZ in the Southern Hemisphere and a northeastward-tilted region from the East China Sea in the Northern Hemisphere. This hemispheric symmetry presumably resulted from the Rossby wave train from the tropics into both hemispheres (Trenberth et al. 1998; Zhang et al. 2014a), and might be a key determinant through which the SSTs in the YECS evolve along with ones in the southern oceans.

[19] The characteristic structures shown in Figures 4d and e − off-equatorial weakened southeasterly trade winds and a meridional SST dipole pattern in the SEP accompanied by the northern lobe of the SPO and its hemispheric symmetry pattern − match exactly the atmospheric-oceanic signatures of the SPMM (Zhang et al. 2014a; Min et al. 2017; Larson et al. 2018; Amaya 2019; see Figure 1b of Zhang et al. 2014a), which is known as a precursor of the EP El Niño (Zhang et al. 2014a; Min et al. 2017; You and Furtado 2017) or a modulator of the ENSO's amplitude (Imada et al. 2016; Larson et al. 2018). This EP Niño signature generally overwhelms this meridional mode; therefore, the SPMM by itself is analogous to a typical El Niño-like pattern particularly in the presence of ocean involved dynamics within the equatorial Pacific (Zhang et al. 2014a; Min et al. 2017; You and Furtado 2017).

3.3 Atmospheric fields in association with the SPMM index

[20] Figure 5 shows the same regressed fields as in Figure 4, but on the standardized MJJ SST anomaly averaged over the SEP region. We defined this time series as the SPMM index. After the

regime shift, the general patterns of the regressed fields, as expected, were almost identical to those regressed onto the YECE SST index because the two indices were coherent during this period, as shown in Figure 2b. The SPMM tends to render an El Nino-like pattern before the regime shift, as expected from previous studies (Figures 5a and b). The convergence of regressed winds east of 150°E is accompanied by reinforced precipitation and warm SST anomalies over the central to eastern equatorial Pacific (Figure 5a-c). Concurrently, a subtropical high-pressure system juxtaposed with robust depressed precipitation has appeared in the western North Pacific. This spatial structure has a typical southwest-northeast tilted wNPSH pattern, whose northern rim delimits the southern boundary of the YECS around 30°N, implying a limited influence of the equatorial signature on the YECS SST anomalies.

[21] Owing to the similarity between the SPMM and ENSO, studies on the meridional modes have devoted substantial efforts to remove the ENSO signals, for instance, by adopting linear regression to separate the cold tongue index from the reanalysis dataset (Chiang and Vimont 2004; Min et al. 2017); by coupling a slab ocean mixed layer model to remove oceanic dynamics, thus pulling apart the Bjerknes feedback and Rossby wave adjustments (Zhang et al. 2014a); by prescribing climatological winds which have no anomalous ENSO-related forcing to the ocean model (Larson et al. 2018; Zhang et al. 2021). We do not attempt to remove the oceanic dynamics, and the ENSO-like signature before the regime shift is unsurprising. However, the independent SPMM pattern after the regime shift is quite intriguing. The obvious emergence of the SPMM signature in recent years might hint that the amplitude of the canonical ENSO might have been substantially reduced after the early 2000s, as several articles have argued (e.g., McPhaden 2012; Kohyama et al. 2017; Li et al. 2019). This hypothesis is further investigated in the following section.

3.4 SPMM-related modes before and after the regime shift

[22] To investigate what has changed systematically in the tropical Pacific and western North Pacific, an SVD analysis was applied to a cross-covariance matrix between the MJJ SST in the domain of the tropical Pacific (20°S-20°N/140°E-70°W) and the MJJ precipitation in the western Pacific (20°S-50°N/110°E-150°W) to extract the leading variability for the respective periods by following Yim et al. (2008). Figure 6 illustrates the SPMM-related SVD modes and their corresponding principal components: the primary mode for the period before the regime shift and the third mode for the period after the regime shift based on the fact that the SPMM index covaried with the PC1s for the early period and the PC3 for the recent period (see Figures 6b and 6e). The correlations between the SPMM index and SST PC1 for the early period and SST PC3 for the recent period are –0.61 and 0.78, respectively; these correlations are significant at a 95% confidence level.

[23] The SST spatial pattern of the primary mode during the early years had a cold tongue pattern that extended from the equatorial eastern Pacific, indicating this mode was also related to the EP El Niño (i.e., the correlation between the SST PC1 and Nino3 index was –0.98), and its corresponding rainfall pattern was a typical southwest-northeast tilted pattern of the wNPSH. The correlation between the principal components of the SST and precipitation was 0.92, suggesting a strong coupling between the EP El Niño-like pattern and precipitation over the western North Pacific. Besides, the analogy between Figures 6a and 4b might demonstrate that the EP El Niño-related wNPSH partially determined the East Asian summer monsoon during the period before the regime shift in agreement with previous findings such as those by Yim et al. (2009) and Wang et

al. (2013). This primary EP El Niño-wNPSH coupling mode explains approximately half (48.5%) of the square covariance between the two fields.

[23] The primary mode for the period 2003–2020 was also an El Niño-like pattern, but with extra loading in the central equatorial Pacific, and its corresponding rainfall pattern changed with increased precipitation sitting over the western Pacific warm pool instead of over the wNPSH region, as reported by Yim et al. (2008) (not shown). Noteworthy was a substantial decrease in the square covariance: the SVD1 during the recent period only accounted for 31.0% of the square covariance between the two time series, which was an approximately 20% decrease in the explained percentage by the primary mode during the period before the regime shift. The SPMM-related pattern appeared in the third mode during the recent period (Figure 7d-f). While this mode's contribution to the total variability was 14.3%, a robust correlation higher than 0.80 between the PCs of SST and precipitation demonstrated a close coupling between the SST over the SEP and the rainfall in the western North Pacific. Intriguingly, the rainfall pattern of SVD3 (Figure 7d) had a meridionally dipole pattern in the western tropical Pacific and depressed precipitation over the YECS, which was quite similar to the regressed rainfall patterns on the YECS SST index (Figure 5e) and the SPMM index (Figure 6e). This result indicates that the ocean and atmospheric signals appearing in the western North Pacific, including the YECS, could be a large-scale atmospheric response to tropical precipitation changes (Deser and Phillips 2006; He et al. 2011; Wu et al. 2015; Liu et al. 2018) triggered by tropical SST and amplified by the ocean-atmospheric dynamic coupling (Okumura 2013; Song and Zhang 2016). The SVD analysis and regression analysis in Figure 5 and previous articles, collectively confirm that the SPMM had an ENSO-like signature, but for the period 1982−2002. The situation seems to have changed throughout the early 2000s.

The SPMM appeared as an independent mode, as the dominant El Niño signature has been substantially weakened, which hints that the mean state of the tropical Pacific might be a La Niña-like condition, as we will discuss in the next section.

4. Discussion

4.1. La Niña-like state during the post-2003 regime

[25] To elucidate the systematic change in the tropical Pacific during the early 2000s, we have estimated the epoch differences between two periods, i.e., the recent period of 2003–2020 minus the early period of 1981–2002 for SST, zonal winds at an 850 hPa level, and precipitation (Figure 7). As the YECS summer SST is closely related to the SEP anomalies for extended months, as depicted in Figure 3, we show the mean differences averaged for the months from February to July. These spatial patterns of epoch difference are not sensitive to the selection of the months. The SST difference shows that the western tropical Pacific warms more than the eastern tropical Pacific, with the highest warming of up to 0.8°C being located in the southwestern tropical Pacific centered around the dateline. Weak but cold anomalies appear over the cold tongue region and the SEP off the coast of Chile, and over the northeast subtropical Pacific off the Californian coast toward the central equatorial Pacific. This SST difference pattern coincided with trade winds that strengthened by 12.5% relative to the period before the regime shift (the red box in Figure 7b). The zonal precipitation gradient was also enhanced by 22.3% (Figure 7c) around the central equatorial Pacific. These results reflect that the Walker Circulation was intensified for the post-2003 period relative to the previous period, suggesting a La Niña-like mean state. The shift from

an El Niño-like to a La Niña-like regime might have been related to the resultant modulation of the weakened air-sea thermodynamic coupling over the SEP during the post-2003 era.

[26] The strength of El Niño events tends to fluctuate substantially, while that of La Niña remains flat (Kohyama et al. 2017). This nonlinear characteristic of the ENSO means that an inactive ENSO for a specific period can be understood as the tropical mean state being rectified to become La Nina-like, and vice versa (An and Jin 2004). The ENSO activity, therefore, can be illustrated with a sliding standard deviation for the ENSO indices, as demonstrated by Kohyama et al. (2017). Figure 8 presents the February to July mean Nino3 SST index (the grey line) and its nine-year sliding standard deviation (the black dashed line). The sliding standard deviation of the Nino3 index for the early years was higher than 0.7, and then reduced drastically to around 0.3 during the early 2000s, indicating that the background tropical Pacific state shifted suddenly from an El Niño-like to a La Niña-like regime. This result is consistent with the explained squared covariance by the SVD1, showing that the EP El Niño-like pattern was substantially reduced from 48.5% to 31%, as noted in the above section.

[26] The shift from the El Niño-like to the La Niña-like regime might have been related to the resultant modulation of the weakened air-sea thermodynamic coupling over the SEP during the post-2003 era. Song and Zhang (2016) prescribed a cold SST anomaly within the SEP to remedy the double ITCZ problem that has frequently emerged in coupled climate models. Their experiment consequently projected an anomalous descending motion via the southeasterly wind anomalies over the SEP which concurrently decreased precipitation, and then, in turn, intensified sea surface cooling through increased evaporation. The interaction of cold SST anomalies with low-level off-equatorial winds over the SEP could have constituted the positive feedback and

reflected a forcing role of the cold SEP SST anomaly in driving the La Niña-like mean state as a low-frequency response. This long-term modulation of the ENSO-mean state reminds us of a positive to negative phase shift of the Interdecadal Pacific Oscillation (IPO), the leading mode of the TPDV (Okumura et al. 2017), in around the year 2000 (e.g., Dong and Dai 2016; Hu et al. 2017; Li et al. 2019). The decadal phase shift inferred from our analysis is also consistent with evidence from previous studies that have demonstrated an overall weakening of the thermodynamical variability in the eastern equatorial Pacific in recent years (Hu et al. 2017), including the decreased transport of oceanic heat from the western warm pool region to the eastern equatorial Pacific via suppressed oceanic Kelvin waves in association with both a weakening of the low-level westerly winds (or a westward shift of the atmosphere-ocean coupling) in the central and eastern tropical Pacific (Li et al. 2019), reduced oceanic thermocline feedback (Guan and McPhaden, 2016), and intensified thermal stratification within the upper ocean in the eastern equatorial Pacific (Imada et al. 2016; Hu et al. 2017; Kohyama et al. 2017). It is noteworthy that the standard deviation of the Nino3 SST index has gradually bounced back in recent years, as shown in Figure 9, presumably reflecting the gradually weakening YECS-SEP coupling in recent years, as shown in Figure 2c. The hypothesis that the tropical Pacific mean state could determine the interhemispheric teleconnection might be in line with the asymmetric teleconnection of the ENSO forcing associated with the IPO's phase (Dong and Dai 2015; Dong et al. 2018), which needs further research.

4.2 An atmospheric bridge for the interhemispheric connection

[27] An important question that needs to be answered is how the air-sea variability signal in the SEP could have crossed the equator and reached the extratropics of the Northern Hemisphere in recent years. Many previous studies have argued that interhemispheric teleconnection is likely determined through modulating precipitation around the ITCZ (e.g., Trenberth et al. 1998; Deser and Phillips 2006; Zhang et al. 2014b; Ding et al. 2015; Wu et al. 2015; Liu et al. 2018). Besides, the fact that the ITCZ is located north of the equator at around 7°N for most of the year allows the propagation of the SEP signals onto the central to western equator through the WES and shallow wind-driven meridional circulation (Gu and Philander 1997; Okumura 2013; Zhang et al. 2014a;b), thus likely resulting in convective precipitations in the western tropical Pacific. Figure 9 shows the lagged regression of anomalous components for convective (left column) and large-scale (right) precipitation onto winter (JFM) mean SST anomalies in the SEP region. The selection of the JFM months is based on the significant relationship of the MJJ mean SEP SST anomalies to one for these months, as illustrated in Figure 3. As we expected from the SVD analysis above, increased precipitation throughout the region between the ITCZ and SPCZ, along with the accompanying compensated suppressed precipitation over the convergence zones, are remarkable in the regressed fields for the convective component (see Figures 9a-j). The maximum convective precipitation anomalies appeared for a one- or two-month lagged field (Figure 9b-c) and seemed to last until the summer months (Figure 9e). This result demonstrates that the convective precipitation changes in the western tropical Pacific followed SST variance within the SEP by one or two months. As an extratropic response to the convective precipitation over the tropical Pacific, the large-scale precipitation component appeared to decrease over the western North Pacific, and finally over the YECS in the spring and summer months (Figures 9i-k).

[28] To explore the detailed role of the atmospheric bridge of tropical precipitation in transferring the SEP signals to the Northern Pacific, we quantitatively portray the precipitation index as the difference in the standardized winter (JFM) average convective precipitation between the two boxes, as shown in Figure 9a (red minus blue boxes). Figure 10 illustrates the regression fields of the low-level (i.e., 1000 hPa) divergence anomaly of the winds with a superposed 850 hPa geopotential height anomaly onto the winter SPMM index – the SST anomaly over the SEP – (left-hand column in Figure 10) and onto the precipitation index (right-hand column). It is immediately apparent that the large-scale atmospheric responses to the SEP SST anomalies in the Northern Hemisphere (Figure 10a) were quite analogous to those for the convective precipitation in the tropical Pacific (Figure 10f) with negative geopotential height signals in the extra-tropics in both hemispheres and a positive one over the western Pacific. This result hints that the precipitation anomaly in the western tropical Pacific could have acted as an atmospheric bridge between the SEP and the northwestern Pacific. A close inspection reveals that the response to the SPMM in the Northern Hemisphere had a maximum for a one-month lagged field (Figure 10b), while the one for the western tropical convective precipitation appeared with a zero-month lag. Our interpretation is that the air-sea interactive signals over the SEP region seem to have reached the equator in one month, then spontaneously modulated large-scale atmospheric circulation in the Northern Hemisphere by altering the western tropical precipitation. This anomalous low-level convergence (or upper tropospheric divergence) in the tropics and divergence in the subtropics, as shown in Figure 10, could have acted as a Rossby wave source with an alternate stream function emanating from the western Pacific over both hemispheres (Trenberth et al. 1998; Terray 2011;

Zhang et al. 2014a). This wave response will be discussed in a future paper based on linear baroclinic model experiments.

[29] An intriguing feature which comes from comparing the figures in the left-hand column with those in the right-hand column in Figure 10, is that the regressed fields driven from the SST anomaly over the SEP persisted for a longer period than those from the precipitation index over the western tropical Pacific. This observation was due to the large thermal inertia of the ocean, indicating an ocean-atmospheric thermodynamic coupling of the SEP SST anomaly (Zhang et al. 2014a; Min et al. 2017).

5. Summary and concluding remarks

[30] This paper was motivated by an attempt to explain why the reported ENSO-induced YECS SST modulation was weak and a forcing region inconsistent in the literature. We have explored this question by assuming a decadal change in the mean state of the tropical Pacific in around the early 2000s and the existence of the ENSO's precursor, i.e., the meridional modes. Consistent with these hypotheses, we found a shift in the decadal relationship between the summer (MJJ) mean SST in the YECS and tropical Pacific anomalies for the period 1982–2020 (Figure 2).

[31] During the period before the early 2000s, a canonical EP El Niño-like signature was prevalent and overwhelmed the air-sea interacted variability in the southeastern tropical Pacific (SEP) – South Pacific Meridional Mode (SPMM); the ENSO-related western North Pacific Subtropical High (wNPSH; Wang et al. 2013) seemed to partially regulate the meridional winds and precipitation over the EASM region. This ENSO-related atmospheric modulation in the western North Pacific, however, had an insignificant effect on the SST in the YECS. On the other hand,

during the post-2003 era, when the mean state of the equatorial Pacific reverted to being La Niño-like, the SPMM, characterized by an off-equatorial wind-induced SST anomaly associated with an anomalous South Pacific subtropical high, appeared to be an independent mode from the ENSO. We believe that the convective precipitation over the western tropical Pacific acted as an atmospheric bridge to mediate this interhemispheric teleconnection and induced an upward motion in the troposphere, resulting in increased convective precipitation between the ITCZ and SPCZ regions and suppressed rainfall over these convergence zones. This convective forcing might have rendered Rossby-wave patterns in the extratropical regions in both hemispheres (Trenberth et al. 1998), thus causing hemispheric symmetric patterns in geopotential height and precipitation fields, as argued by Zhang et al. (2014a).

[32] The reason an apparently SST signature for the SPMM appeared over the YECS is unclear, since the SPMM-related, most remarkable pressure system in the Northern Hemisphere was located near the Aleutian Islands (Figure 4b). Compared to the deep open ocean, where intrinsic variability is more important due to its large thermal inertia, the shallow water of the YECS (its mean depth is only 75m) can increase its susceptibility to climate forcing. Despite the debatable role of the discharged riverine waters on the YECS SST, the change in precipitation-induced riverine waters associated with the SPMM might have amplified the atmospheric forced SST variability, especially from May to July, through their horizontal advection as an instantaneous response (Belkin 2009; Park et al. 2011; Kako et al. 2016).

[33] Our results have implications for the predictability of the strength of the EASM, which modulates weather, intense summer precipitation, tropical storms, and marine heatwaves (Wang et al. 2013; Zhang et al. 2016), thus having a broad socio-economic impact on the western North

Pacific. The robust relationship presented here between the two seasons preceding the SPMM and the EASM, particularly during the inactive ENSO period, complements the well-known relationship between the wNPSH and EASM (Wang et al., 2013) and could drive a more concrete, empirical prediction model.

[36] The present study focused on the interannual variance of the SPMM due to a lack of reliable multidecadal SST time series. Previous studies, however, have underlined the critical role of stochastic forcing from weather systems in the Southern Hemisphere (Okumura 2013; Liguori and Di Lorenzo 2019; Zhang et al. 2021), in tandem with a subsurface temperature anomaly driven by the subtropical shallow meridional subduction in the SPMM region (Gu and Philander 1997; Imada et al. 2016), on driving decadal ENSO-like variability, IPO. Kohyama and Hartmann (2017) proposed a nonlinear ENSO warming suppression (NEWS) mechanism to show that La Nina-like mean-state warming is also a possible candidate in a warm climate because of the nonlinear rectification effect (Jin et al. 2003). If the NEWS mechanism is pertinent to future projections, SPMM-YECS coupling may become more common with global warming (Ashok et al. 2012; Imada et al. 2016). However, future projections are controversial in climate models. Therefore, the following issues require attention: the future tendencies of the SPMM with global warming; the decadal variation of the SPMM and its impact on climate such as the ENSO's flavor and the global warming hiatus; the decadal evolution of the YECS-SPMM coupling; the cause-effect relationship between the mean state in the tropical Pacific and the frequency of extreme El Nino events.

Acknowledgements

This research is a part of the projects entitled “Establishment of the ocean research station in the jurisdiction zone and convergence research” and “Study on air-sea interaction and process of rapidly intensifying typhoon in the northwestern Pacific” funded by the Ministry of Oceans and Fisheries. YSK is also supported by the National Research Foundation of Korea grant funded by the Korea government (NRF-2020R1F1A1070398). ESC is supported by the Ministry of Oceans and Fisheries, Korea project, entitled “Investigation and Prediction System Development of Marine Heatwave around the Korean Peninsula originated from the Sub-Arctic and Western Pacific” (20190344).

Data availability

The data used in this work are available to download from their developers’ or authorized websites.

Declarations

Conflict of interest The authors declare no knowledge of any conficts of interest that could infuence the publication of this work.

References

Amaya DJ (2019) The Pacific Meridional Mode and ENSO: A Review. Curr Clim Change Rep doi:10.1007/s40641-019-00142-x

An S-I, Jin F-F (2004) Why El Niño is stronger than La Niña. J Clim 17(12):2399–2412

Ashok T, Sabin TP, Swapna P and Murtugudde RG (2012) Is a global warming signature emerging in the tropical Pacific? Geophys. Res. Lett 39:L02701.

Bao B, Ren G (2014) Climatological characteristics and long-term change of SST over the marginal seas of China. Cont Shelf Res 77: 96−106

Beardsley R, Limeburner R, Yu H, Cannon G (1985) Discharge of the Changjiang (Yangtze River) into the East China Sea. Cont Shelf Res 4:57–76

Belkin IM (2009) Rapid warming of large marine ecosystems. Prog Oceanogr 81: 207−213

Bretherton CS, Widmann M, Dymnikov VP, Wallace JM, Bladé I (1999) The effective number of spatial degrees of freedom of a time-varying field. J Clim 12(7):1990–2009

Cai R, Tan H, Kontoyiannis H (2017) Robust surface warming in offshore China Seas and its relationship to the East Asian Monsoon wind field and ocean forcing on interdecadal time scales. J Clim 30:8987–9005. doi: 10.1175/JCLI-D-16-0016.1

Capotondi A, Wittenberg AT, Newman M, Di Lorenzo E, Yu JY, Braconnot P, et al. (2015) Understanding ENSO diversity. Bull Am Meteorol Soc 96:921–938. doi:10.1175/BAMS-D-13-00117.1

Chang P, Zhang L, Saravanan R, Vimont DJ, Chiang JCH, L. Ji, H. Seidel, and M. K. Tippett (2007) Pacific meridional mode and El Niño–Southern Oscillation. Geophys Res Lett 34:L16608. doi:10.1029/2007GL030302

Chiang JCH, Vimont DJ (2004) Analogous Pacific and Atlantic meridional modes of tropical atmosphere-ocean variability. J Clim 17:4143–4158, doi:10.1175/JCLI4953.1

Choi Y, Ha K-J (2018) Subseasonal shift in tropical cyclone genesis over the western North Pacific in 2013. Clim Dyn 51:4451−4467, doi:10.1007/s00382-017-3926-0

Deser C, Phillips AS (2006) Simulation of the 1976/77 climate transition over the North Pacific: Sensitivity to tropical forcing. J Clim 19:6170−6180

Di Lorenzo E, Cobb KM, Furtado JC, Schneider N, Anderson BT, Bracco A, Alexander MA, Vimont DJ (2010) Central Pacific El Niño and decadal climate change in the North Pacific Ocean. Nat Geosci 3:762−765. doi: 10.1038/NGEO984

Dong B, Dai A (2015) The influence of the Interdecadal Pacific Oscillation on Temperature and Precipitation over the Globe. Clim Dyn doi:10.1007/s00382-015-2500-x

Dong B, Dai A, Vuille M, Timm OE (2018) Asymmetric modulation of ENSO teleconnections by the Interdecadal Pacific Oscillation. J Clim 31(18):7737–7361. doi: 10.1175/JCLI-D-17-0663.1

Du Y, Yang L, Xie S-P (2011) Tropical Indian Ocean influence on Northwest Pacific tropical cyclones in summer following strong El Niño. J. Climate 24:315−322

Fan H, Huang H (2008) Response of coastal marine eco-environment to river fluxes into the sea: A case study of the Huanghe (Yellow) River mouth and adjacent waters. Mar Environ Res, 65:378–387.

Fan L, Shin S-I, Liu Q, Liu Z (2013) Relative importance of tropical SST anomalies in forcing East Asian summer monsoon circulation. Geophys Res Lett 40:2471-2477. doi:10.1002/grl.50494

Gu D, Philander GH (1997) Interdecadal climate fluctuations that depend on exchanges between the tropics and extratropics. Science 275:805–807.

Guan C, McPhaden MJ (2016) Ocean processes affecting the twenty- first-century shift in ENSO SST variability. J Clim 29:6861–6879. https://doi.org/10.1175/JCLI-D-15-0870.1

Ha K-J, Heo K-Y, Lee S-S, Yun K-S, Jhun J-G (2012) Variability in the East Asian Monsoon: a review. Meteorol Appl 19:200−215. doi:10.1002/met.1320

Ha K-J, Nam S, Jeong J-Y, Moon I-J, Lee M, Yun J, Jang CJ, Kim YS, Byun DS, Heo K-Y, Shim J-S (2019) Observations utilizing Korea ocean research stations and their applications for process studies. B Am Meteorol Soc doi:10.1175/BAMS-D-18- 0305.1.

Hardiman SC, Dunstone NJ, Scaife AA, Bett PE, Li C, Lu B, Ren H-L, Smith DM, Stephanet CC (2018) The asymmetric response of Yangtze River basin summer rainfall to El Niño/La Niña. Environ Res Lett 13:024015. doi:10.1088/1748-9326/aaa172

He J, Lin H, Wu Z (2011) Another look at influences of the Madden-Julian Oscillation on the wintertime East Asian weather. J Geophys Res 111 D03109. doi: 10.1029/2010JD014787

Hersbach H, Bell B, Berrisford P et al (2020) The ERA5 global reanalysis. Q J R Meteorol Soc doi: 10.1002/qj.3803

Hu Z-Z, Kumar A, Huang B, Zhu J, Ren H-L (2017) Interdecadal variations of ENSO around 1999/2000. J Meterol Res 31: 73–81. doi:10.1007/s13351-017-6074-x

Imada Y, Tatebe H, Watanabe M, Ishii M, Kimoto M (2016) South Pacific influence on the termination of El Niño in 2014. Sci Rep 6:30341. doi:10.1038/srep30341

Jo H-S, Yeh S-W, Lee S-K (2015) Changes in the relationship in the SST variability between the tropical Pacific and the North Pacific across the 1998/1999 regime shift Geophys Res Lett 42:7171−7178. doi:10.1002/2015GL065049

Kako SI, Nakagawa T, Takayama K, Hirose N, Isobe A (2016) Impact of Changjiang River discharge on sea surface temperature in the East China Sea. J Phys Oceanog 46:1735–1750. doi:10.1175/jpo-d-15-0167.1

Kim YS, Jang CJ, Yeh S-W (2018) Recent surface cooling in the Yellow and East China Seas and the associated North Pacific regime shift. Cont Shelf Res 156:43−54, doi: j.csr.2018.01.009

Kohyama T, Hartmann DL, Battisti DS (2017) La Niña–like mean-state response to global warming and potential oceanic roles. J Clim 30:4207–4225. doi:10.1175/JCLI-D-16-0441.1

Kohyama T, Hartmann DL (2017) Nonlinear ENSO warming suppression (NEWS). 30:4227−4251. doi:10.1175/JCLI-D-16-0541.1

Larson SM, Pegion KV, Kirtman BP (2018) The South Pacific meridional mode as a thermally driven source of ENSO amplitude modulation and uncertainty. J Clim 31:5127−5145. doi:10.1175/JCLI-D-17-0722.1

Lau N-C, Nath MJ (1996) The role of the atmospheric bridge in linking tropical Pacific ENSO events to extratropical SST anomalies. J Clim 9:2036–2057

Li X, Hu Z-Z, Becker E (2019) On the westward shift of tropical Pacific climate variability since 2000. Clim Dyn 53:2905–2918, doi:10.1007/s00382-019-04666-8

Liao E, Lu W, Yan X-H, Jiang Y, Kidwell A (2015) The coastal ocean response to the global warming acceleration and hiatus. Sci Rep 5:16630, doi:10.1038/srep16630

Liguori G, Di Lorenzo E (2018) Meridional modes and increasing Pacific decadal variability under anthropogenic forcing. Geophys Res Lett 45. doi:10.1002/2017GL076548

Liguori G, Di Lorenzo E (2019) Separating the North and South Pacific Meridional Modes contributions to ENSO and tropical decadal variability. Geophys Res Let 46:906–915. doi:10.1029/2018GL080320

Lima FP and Wethey DS (2012) Three decades of high-resolution coastal sea surface temperatures reveal more than warming. Nat Commun 3:704 doi:10.1038/ncomms1713

Liu N, Wang H, Ling T, Feng L (2013) The influence of ENSO on sea surface temperature variations in the China seas. Acta Oceanol Sin 32(9):21−29. doi:10.1007/s13131-013-0348-7

Liu T, Li J, Li Y, Zhao S, Zheng F., Zheng J (2018) Influence of the May Southern annular mode on the South China Sea summer monsoon. Clim Dyn 51:4095–4107. doi: 10.1007/s00382-017-3753-3.

McPhaden, MJ (2012) A 21st century shift in the relationship between ENSO SST and warm water volume anomalies. Geophys Res Lett 39:L09706, doi:10.1029/2012GL051826

Newman M, Shin S-I, Alexander MA (2011) Natural variation in ENSO flavors. Geophys Res Lett 38:L14705. doi:10.1029/2011GL047658

Newman M, Alexander MA, Ault TR, Cobb KM, Deser C, Di Lorenzo E, Mantua NJ, Miller AJ, Minobe S, Nakamura H, Schneider N, Vimont DJ, Phillips AS, Scott JD, Smith CA (2016) The Pacific decadal oscillation, revisited. J Clim 29:4399−4427. doi:10.1175/JCLI-D-15-0508.1

North GR, Bell TL, Cahalan RF, Moeng FJ (1982) Sampling errors in the estimation of empirical orthogonal functions. Mon Weather Rev 110(7):699–706

Min Q, Su J, Zhang R (2017) Impact of the South and North Pacific meridional modes on the El Niño–Southern Oscillation: Observational analysis and comparison. J Clim 30:1705–1720 doi:10.1175/JCLI-D-16-0063.1

Overland J, Rodionov S, Minobe S, Bond N (2008) North Pacific regime shifts: Definitions, issues and recent transitions. Prog Oceanogr 77: 92–102. doi:10.1016/j.pocean.2008.03.016

Okumura YM (2013) Origins of tropical Pacific decadal variability: Role of stochastic atmospheric forcing from the South Pacific. J Clim 26:9791–9796. doi:10.1175/ JCLI-D-13-00448.1

Okumura YM, Sun T, Wu X (2017) Asymmetric modulation of El Niño and La Niña and the linkage to tropical Pacific decadal variability. J Clim 30:4705–4730. doi:10.1175/JCLI-D-16-0680.1

Park J-H, Yeo D-E, Lee KJ, Lee H, Lee S-W, Noh S, et al. (2019) Rapid decay of slowly moving Typhoon Soulik (2018) due to interactions with the strongly stratified northern East China Sea. Geophys Res Lett 46. doi:10.1029/ 2019GL086274

Park K-A, Lee E-Y, Chang E, Hong S (2015) Spatial and temporal variability of sea surface temperature and warming trends in the Yellow Sea. J Mar Syst 143:24−38, doi: 10.1016/j.jmarsys.2014.10.013

Park T, Jang CJ, Jungclaus JH, Haak H, Park W, Oh I-S (2011) Effects of the Changjiang river discharge on sea surface warming in the Yellow and East China Seas in summer. Cont Shelf Res 31:15−22, doi:10.1016/j.csr2010.10.012. 1

Park W-S, Oh I-S (2000) Interannual and interdecadal variations of sea surface temperature in the East Asian Marginal Seas. Prog Oceangr 47:191−204

Rayner NA, Parker DE, Horton EB, Folland CK, Alexander LV, Rowell DP, Kent EC, Kaplan A (2003) Global analyses of sea surface temperature, sea ice, and night marine air temperature since the late nineteenth century. J Geophys Res 108(D14):4407. doi:10.1029/2002JD002670

Reynolds RW, Smith TM, Liu C, Chelton DB, Casey KS, Schlax MG (2007) Daily high-resolution-blended analyses for sea surface temperature. J Clim 20:5473–5496. doi: 10.1175/2007JCLI1824.1

Reynolds RW, Chelton DB (2010) Comparisons of daily sea surface temperature analyses for 2007–08. J Clim 23:3545–3562

Seok S-H, Seo K-H (2021) Sensitivity of East Asian summer monsoon precipitation to the location of the Tibetan Plateau. J Clim doi: 10.1175/JCLI-D-21-0154.1

Song F, Zhang G (2016) Effects of southeastern Pacific sea surface temperature on the double-ITCZ bias in NCAR CESM1. J Clim 29:7417–7433. doi:10.1175/JCLI-D-15-0852.1

Stuecker MF, Timmermann A, Jin F-F, McGregor S, Ren HL (2013) A combination mode of the annual cycle and the El Niño/Southern Oscillation. Nat Geosci 6:540–544. doi: 10.1038/NGEO1826

Stuecker MF (2018) Revisiting the Pacific meridional mode. Sci Rep 8:3216 doi:10.1038/s41598-018-21537-0

Terray P (2011) Southern Hemisphere extra-tropical forcing: a new paradigm for El Niño-Southern Oscillation. Clim Dyn 36:2171–2199. doi:0.1007/s00382-010-0825-z

Trenberth K.E, Branstator G.W, Karoly D, Kumar A, Lau N-C, Ropelewski C (1998) Progress during TOGA in understanding and modeling global teleconnections associated with tropical sea surface temperatures. J Geophys Res 103(C7):14291−14324

Vimont DJ, Wallace JM, Battisti DS (2003) The seasonal footprinting mechanism in the Pacific: implications for ENSO. J Clim 16:2668–2675

Wang B, Wu R, Fu X (2000) Pacific–East Asian teleconnection: how does ENSO affect East Asian climate? J Clim 13:1517–1536

Wang B, Zhou X (2008) Climate variation and prediction of rapid intensification in tropical cyclones in the western North Pacific. Meteorol Atmos Phys 99:1−16. doi:10.1007/s00703-006-0238-z

Wang B, Xiang B, Lee J-Y (2013) Subtropical High predictability establishes a promising way for monsoon and tropical storm predictions. P Natl Acad Sci USA 110(8):2718−2722. doi: 10.1073/pnas.1214626110

Wang F (2010) Subtropical dipole mode in the Southern Hemisphere: A global view. Geophys Res Lett 37:L10702. doi:10.1029/2010GL042750

Wang F, Meng Q, Tang X, Hu D (2013) The long-term variability of sea surface temperature in the seas east of China in the past 40 a. Acta Oceanol Sin 32(3): 48−53. doi:10.1007/s13131-013-0288-2

Wang J, Oey L-Y (2014) Inter-annual and decadal fluctuations of the Kuroshio in East China Sea and connection with surface fluxes of momentum and heat. Geophys Res Lett 41:8538–8546. doi:10.1002/2014GL062118

Wu R, Lin J, Li B (2016) Spatial and Temporal Variability of Sea Surface Temperature in Eastern Marginal Seas of China. Adv Meteorol 2015:3820720. doi:10.1155/2016/3820720

Wu Z, Dou J, Lin H (2015) Potential influence of the November–December Southern Hemisphere annular mode on the East Asian winter precipitation: a new mechanism. Clim Dyn 44:1215−1226. doi: 10.1007/s00382-014-2241-2

Xiang B, Wang B, Yu W, Xu S (2013) How can anomalous western North Pacific Subtropical High intensify in late summer? Geophys Res Lett 40:2349−2354. doi:10.1002/grl.50431

Xie P, Arkin PA (1997) Global precipitation: A 17-year monthly analysis based on gauge observations, satellite estimates, and numerical model outputs. Bull Am Meteorol Soc 78:2539–2558

Xie S-P, Kosaka Yu, Du Y, Hu K, Chowdary JS, Huang G (2016) Indo-Western Pacific Ocean Capacitor and Coherent Climate Anomalies in Post-ENSO Summer: A Review. Adv Atmos Sci 33(4):411-432. doi:10.1007/s00376- 015-5192-6.

Yang F, Lau K-M (2004) Trend and variability of China precipitation in spring and summer: linkage to sea-surface temperatures. Int J Climatol 24:1625–1644. doi:10.1002/Joc.1094

Yeh S-W, Kug J-S, Dewitte B, Kwon M-H, Kirtman B, Jin F-F (2009) El Niño in a changing climate. Nature 461. doi:10.1038/nature08316

Yeh S-W, Kim C-H (2010) Recent warming in the Yellow/East China Sea during winter and the associated atmospheric circulation. Cont Shelf Res 30:1428−1434

Yeh S-W, Wang X, Wang C, Dewitte B (2015) On the relationship between the North Pacific climate variability and the central Pacific El Niño. J Clim 28:663–677. doi:10.1175/JCLI-D-14-00137.1

Yeo S-R, Kim K-Y, Yeh S-W, Kim W-M (2012) Decadal changes in the relationship between the tropical Pacific and the North Pacific. J Geophys Res 117:D15102. doi:10.1029/2012JD017775

Yeo S-R, Kim K-Y (2014) Global warming, low-frequency variability, and biennial oscillation: an attempt to understand the physical mechanisms driving major ENSO events. Clim Dyn 43:771−786. doi:10.1007/s00382-013-1862-1

Yim S-Y, Jhun J-G, Yeh S-W (2008) Decadal change in the relationship between east Asian–western North Pacific summer monsoons and ENSO in the mid-1990s. Geophys Res Lett 35:L20711. doi:10.1029/2008GL035751

You Y and Furtado JC (2017) The role of South Pacific atmospheric variability in the development of different types of ENSO. Geophys Res Lett 44:7438–7446. doi:10.1002/2017GL073475

Zhang L, Wu L, Lin X, Wu D (2010) Modes and mechanisms of sea surface temperature low-frequency variations over the coastal China seas. J Geophys Res 115:C08031, doi:10.1029/2009JC006025

Zhang H, Clement A, Di Nezio P (2014a) The South Pacific meridional mode: A mechanism for ENSO-like variability. J Clim 27:769–783. doi:10.1175 /JCLI-D-13-00082.1

Zhang, H., Deser C, Clement A, Tomas R (2014b), Equatorial signatures of the Pacific Meridional Modes: Dependence on mean climate state. Geophys Res Lett 41:568–574. doi:10.1002/2013GL058842

Zhang W, Li H, Jin F-F, Stuecker M, Turner A, Klingamam N (2015) The annual-cycle modulation of meridional asymmetry in ENSO's atmospheric response and its dependence on ENSO zonal structure. J Clim 28:5795–5812. doi:10.1175/ JCLI-D-14-00724.1

Zhang W, Jin F-F, Stuecker MF, Wittenberg AT, Timmermann A, Ren H-L, Kug J-S, Cai W, Cane M (2016) Unraveling El Niño's impact on the East Asian Monsoon and Yangtze River summer flooding. Geophys Res Lett 43:11,375–11,382. doi:10.1002/ 2016GL071190

Zhang Y., Yu S., Amaya D.J., Kosaka Y., Larson S.M., Wang X., Yang J.-C., Stuecker M.F., Xie S.-P., Miller A.J., and Lin X. (2021) Pacific meridional modes without equatorial Pacific influence. J Clim 34(13):5285−5301, doi:10.1175/JCLI-D-20-0573.1

List of figures

Figure 1. (a) The spatial distribution of the early summer (MJJ) mean SST (shading) for the period 1982−2020, and (b) its time series averaged over the Yellow and East China Seas (YECS; 117−129.5°E/26−41°N), which is defined as the YECS summer SST index. The thin contours in (a) are the 50 m (tan), 100 m (blue), and 2,000 m (black) isobaths. The thick dashed line is the 1.15-m sea surface height to represent the mean path of the Kuroshio by following Wang and Oey (2014). The black star in the central YECS represents the Ieodo Ocean Research Station (I-ORS).

Figure 2. (a) Map of the simultaneous correlation coefficients between the YECS summer SST index and SST anomalies in the Pacific and Indian Oceans for the period 1982−2020. Only the correlations above the 90% confidence level are shaded. (b) Time series of the YECS summer SST index (black bars) and SST anomalies averaged over the Southeastern Pacific (SEP; 130−100°W/20−10°S, red line). The nine-year moving correlation coefficients between the YECS summer SST index and SEP SST anomalies are illustrated in (c), with the central year of each moving period plotted on the x-axis. The dots represent the correlations that are statistically significant at a 95% confidence level.

Figure 3. Maps of lagged correlation coefficients between the early summer (MJJ) YECS SST index and lagged SST anomalies for the separated periods of (a) 1982−2002 and (b) 2003−2020. Only the correlations above the 90% confidence level are shaded. The numbers in parentheses are lagged months.

Figure 4. Regressed anomalies of (a) SST (color), wind (vector), (b) geopotential height (contour) at 850 hPa, precipitation (shading), (c) and meridional wind at the dateline on the YECS summer SST index for the period 1982−2002. (d-f) Same as (a-c), but for the period 2003–2020. The contour interval for the geopotential height anomalies at 850 hPa is 4-m, the negative contours are dashed, and the zero contour is omitted.

Figure 5. Same as Figure 4, but for regression onto the MJJ mean Southeastern Pacific SST anomalies.

Figure 6. Spatial structures of SVD1 between the MJJ mean precipitation anomalies over the region 20°S−50°N, 110°E−150°W and the tropical Pacific SST anomalies over the region 20°S−20°N, 140°E−70°W for (a) precipitation, (c) SST, and their (b) corresponding principal components during the period 1982−2002. (d, e, and f) Same as Figures 7a, 7b, and 7c, respectively, except SVD3 for the period 2003−2020. The red lines in Figures 7b and 7e are the MJJ mean SST anomalies over the Southeastern Pacific (SEP: 20−10°S, 130°−100°W).

Figure 7. Epoch difference map of the February−July mean (a) SST from OISSTv2, (b) zonal wind at 850 hPa from ERA5, and (c) precipitation from the CMAP, obtained by subtracting the period 1982−2002 from the period 2003−2020. The epochal differences in the zonal wind and zonal precipitation gradient are estimated over the regions in the red boxes in (b) and (c), respectively.

Figure 8. February to July mean Nino3 time series (solid gray line) and its nine-year running standard deviation (dashed black line).

Figure 9. Lagged linear regression of the (left) convective (right) large-scale components of the precipitation on the JFM mean SST anomalies over the SEP region for the post-2003 period. The boxes in (a) indicate the domains for the precipitation index in Figure 10.

Figure 10. Lagged linear regression of the divergence of 1000 hPa winds (shading: unit s-1) and geopotential height anomalies at 850 hPa (contour) on the JFM mean (left) SEP index and (right) precipitation index for the post-2003 period. The SEP index is estimated for the mean SST over the red box domain in (a), and the precipitation index for the mean convective precipitation difference between the red and the blue boxes in (f). The contour interval for the geopotential height anomalies is 6 m, the negative contours are dashed, and the zero contour is the thick line.

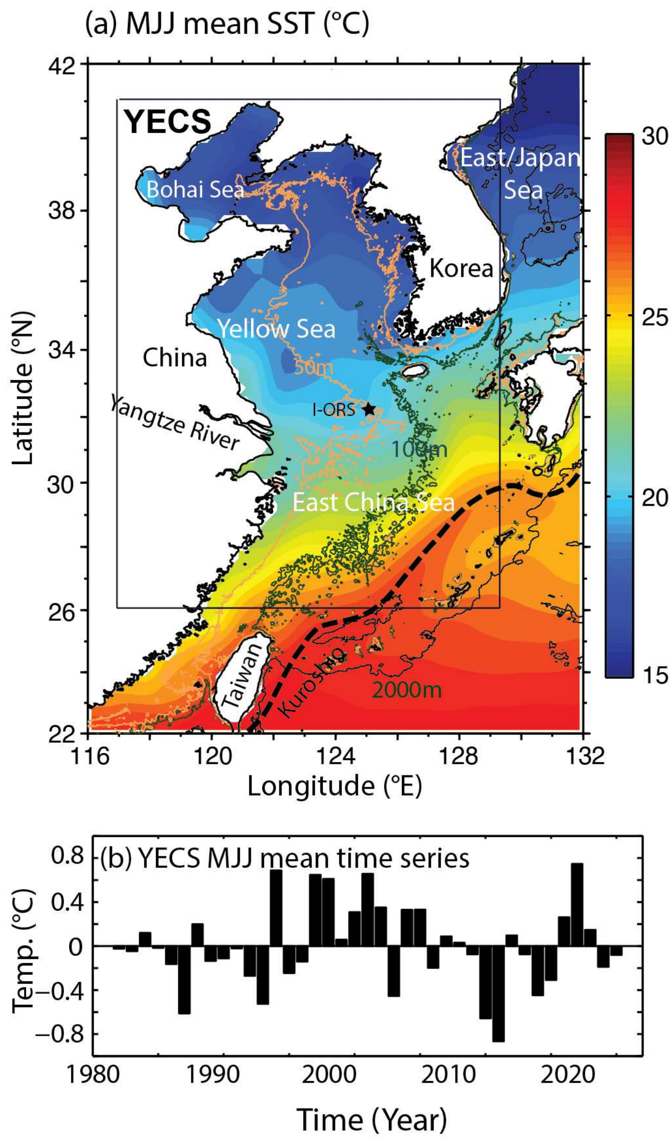

Figure 1. (a) The spatial distribution of the early summer (MJJ) mean SST (shading) for the period 1982−2020, and (b) its time series averaged over the Yellow and East China Seas (YECS; 117−129.5°E/26−41°N), which is defined as the YECS summer SST index. The thin contours in (a) are the 50 m (tan), 100 m (blue), and 2,000 m (black) isobaths. The thick dashed line is the 1.15-m sea surface height to represent the mean path of the Kuroshio by following Wang and Oey (2014). The black star in the central YECS represents the Ieodo Ocean Research Station (I-ORS).

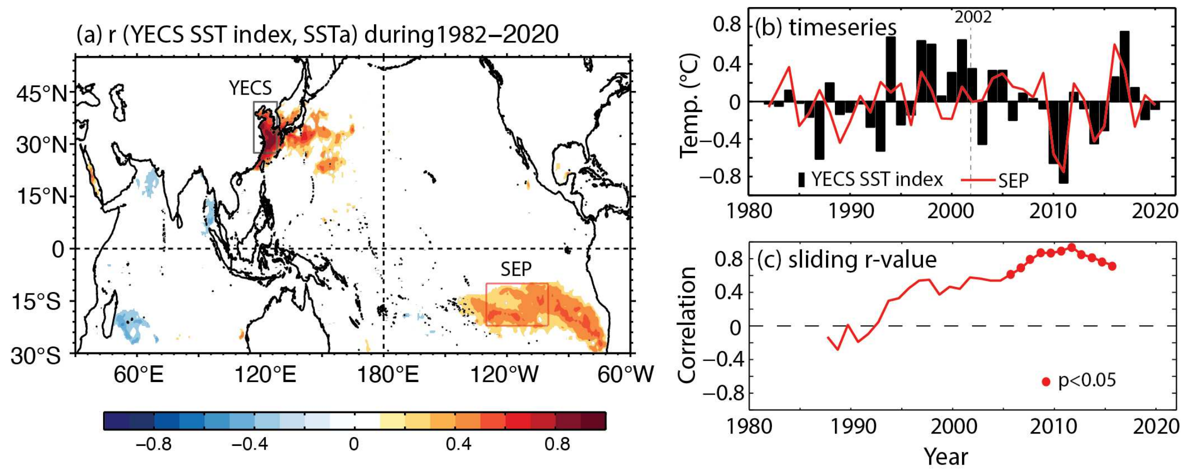

Figure 2. (a) Map of the simultaneous correlation coefficients between the YECS summer SST index and SST anomalies in the Pacific and Indian Oceans for the period 1982−2020. Only the correlations above the 90% confidence level are shaded. (b) Time series of the YECS summer SST index (black bars) and SST anomalies averaged over the Southeastern Pacific (SEP; 130−100°W/20−10°S, red line). The nine-year moving correlation coefficients between the YECS summer SST index and SEP SST anomalies are illustrated in (c), with the central year of each moving period plotted on the x-axis. The dots represent the correlations that are statistically significant at a 95% confidence level.

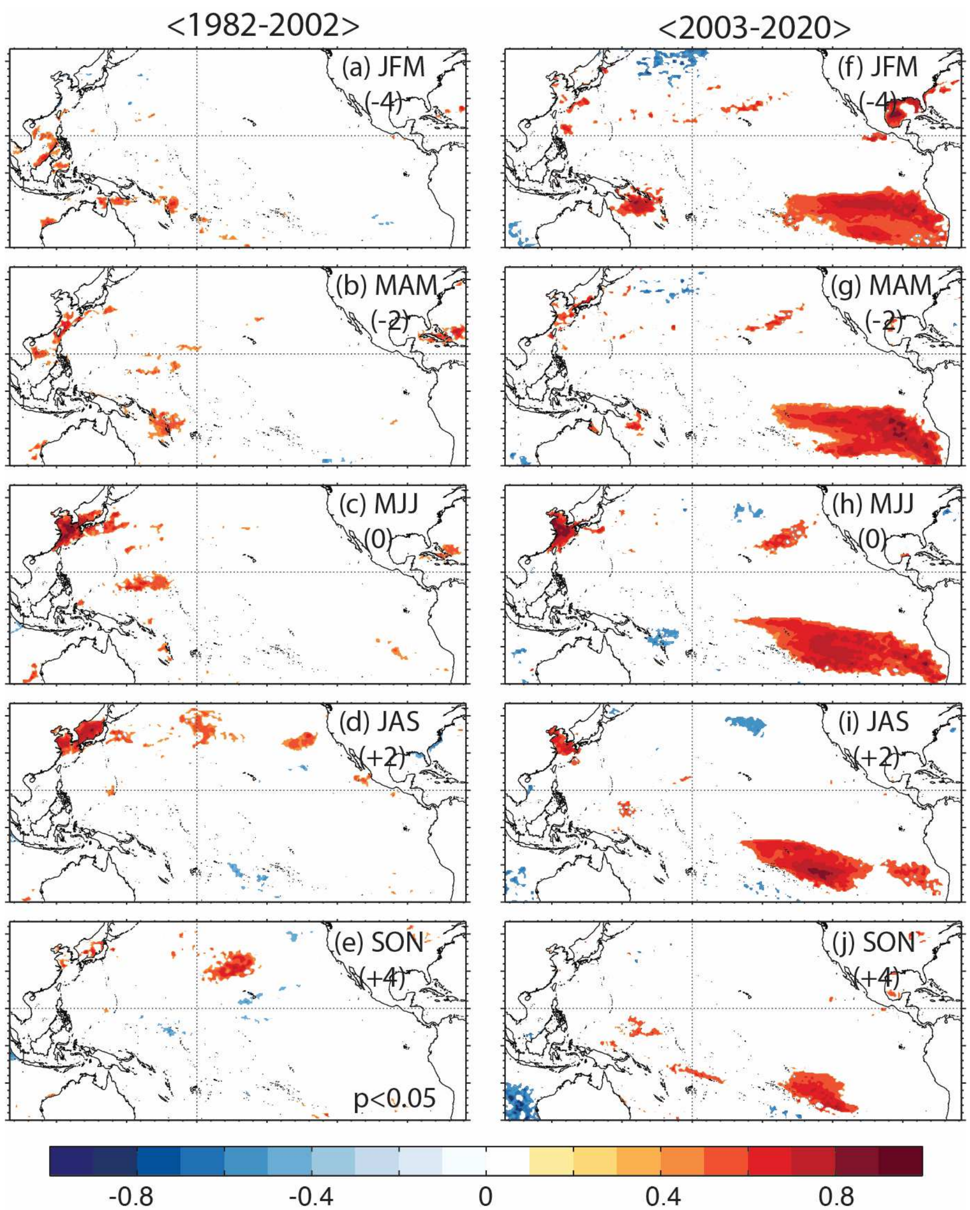

Figure 3. Maps of lagged correlation coefficients between the early summer (MJJ) YECS SST index and lagged SST anomalies for the separated periods of (a) 1982−2002 and (b) 2003−2020. Only the correlations above the 90% confidence level are shaded. The numbers in parentheses are lagged months.

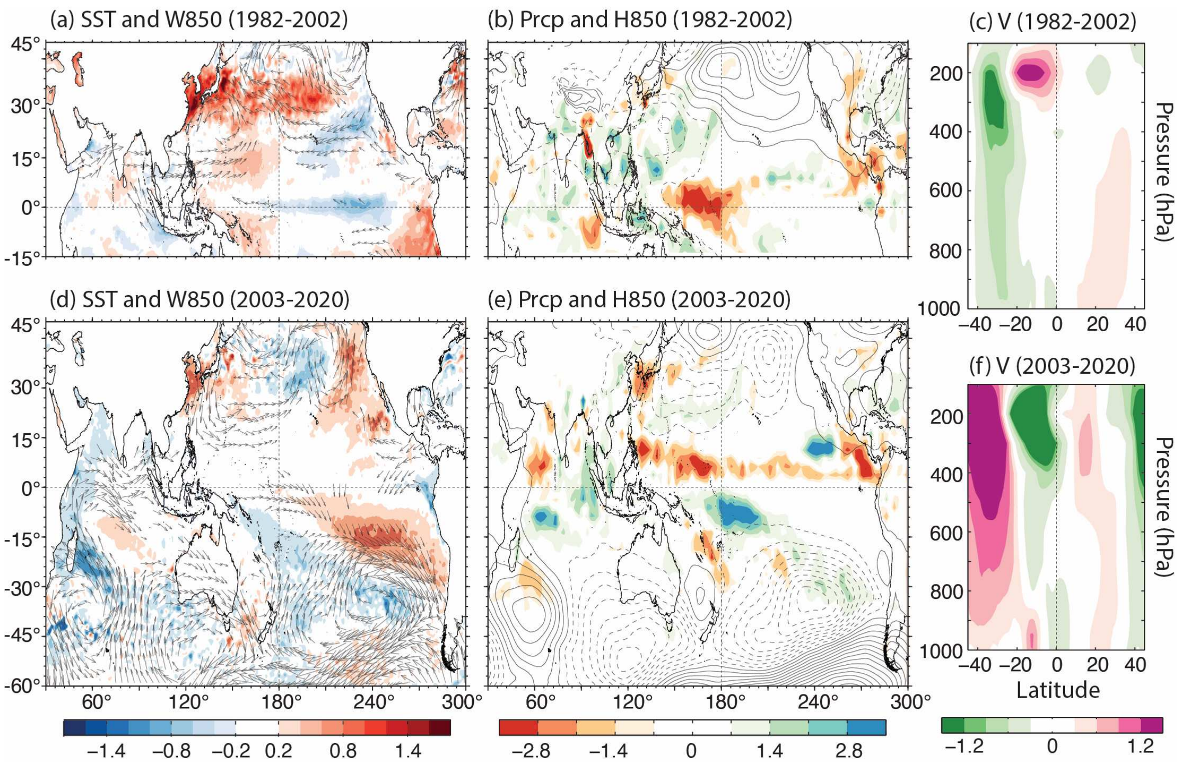

Figure 4. Regressed anomalies of (a) SST (color), wind (vector), (b) geopotential height (contour) at 850 hPa, precipitation (shading), (c) and meridional wind at the dateline on the YECS summer SST index for the period 1982−2002. (d-f) Same as (a-c), but for the period 2003–2020. The contour interval for the geopotential height anomalies at 850 hPa is 4-m, the negative contours are dashed, and the zero contour is omitted.

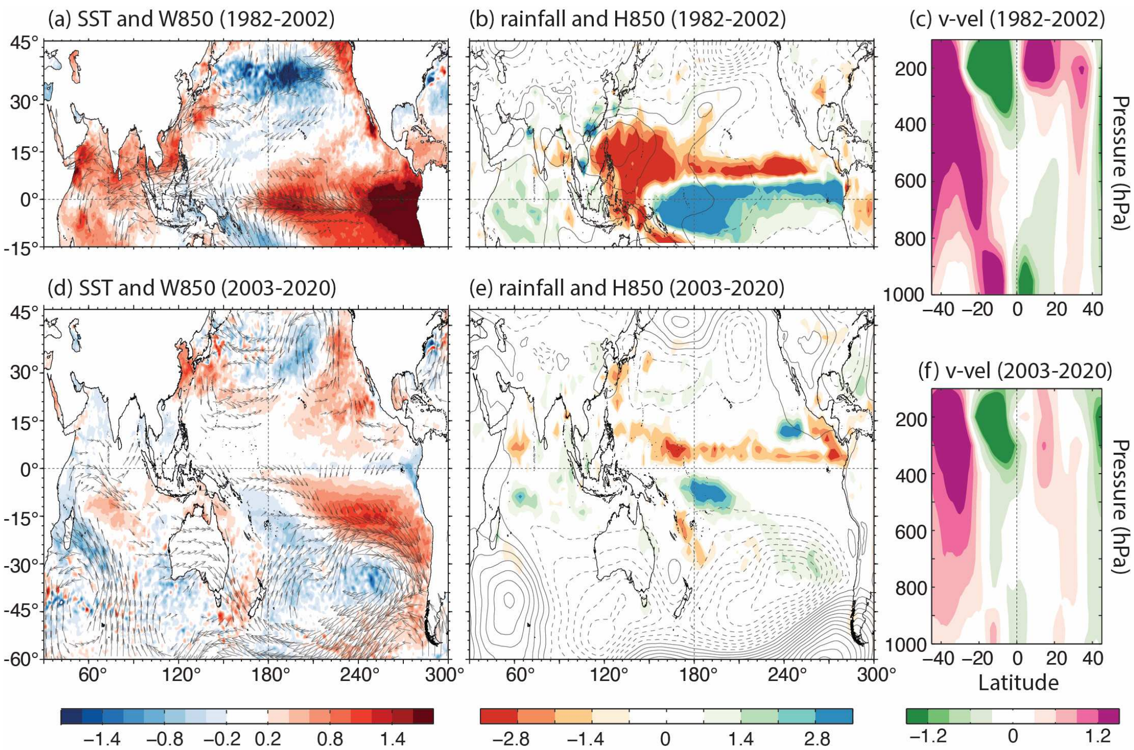

Figure 5. Same as Figure 4, but for regression onto the MJJ mean Southeastern Pacific SST anomalies.

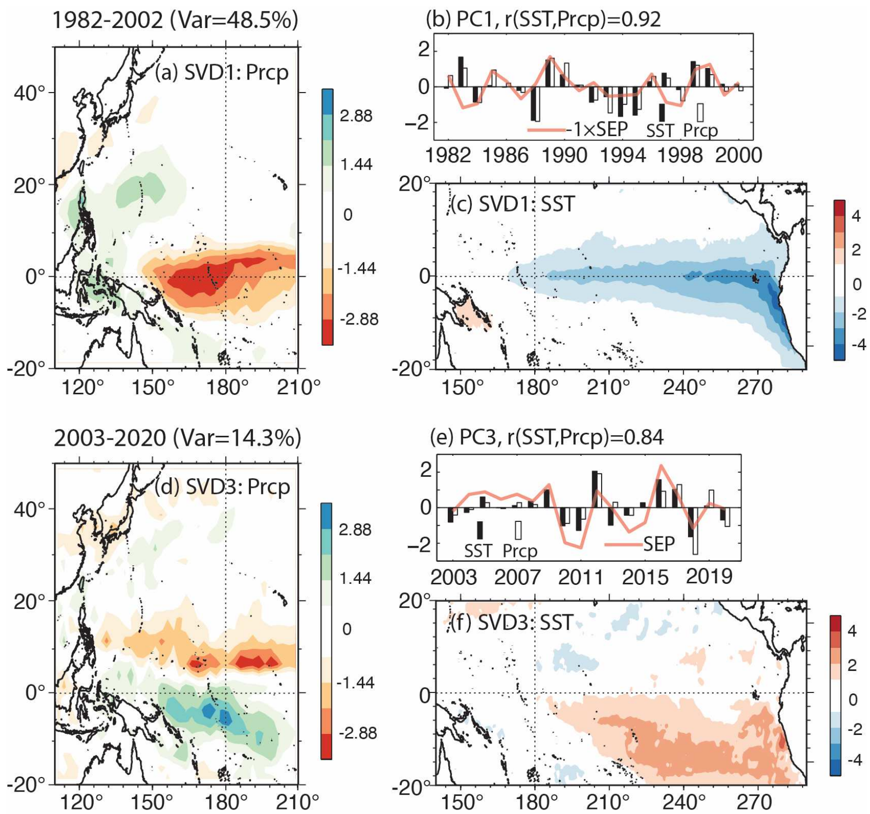

Figure 6. Spatial structures of SVD1 between the MJJ mean precipitation anomalies over the region 20°S−50°N, 110°E−150°W and the tropical Pacific SST anomalies over the region 20°S−20°N, 140°E−70°W for (a) precipitation, (c) SST, and their (b) corresponding principal components during the period 1982−2002. (d, e, and f) Same as Figures 7a, 7b, and 7c, respectively, except SVD3 for the period 2003−2020. The red lines in Figures 7b and 7e are the MJJ mean SST anomalies over the Southeastern Pacific (SEP: 20−10°S, 130°−100°W).

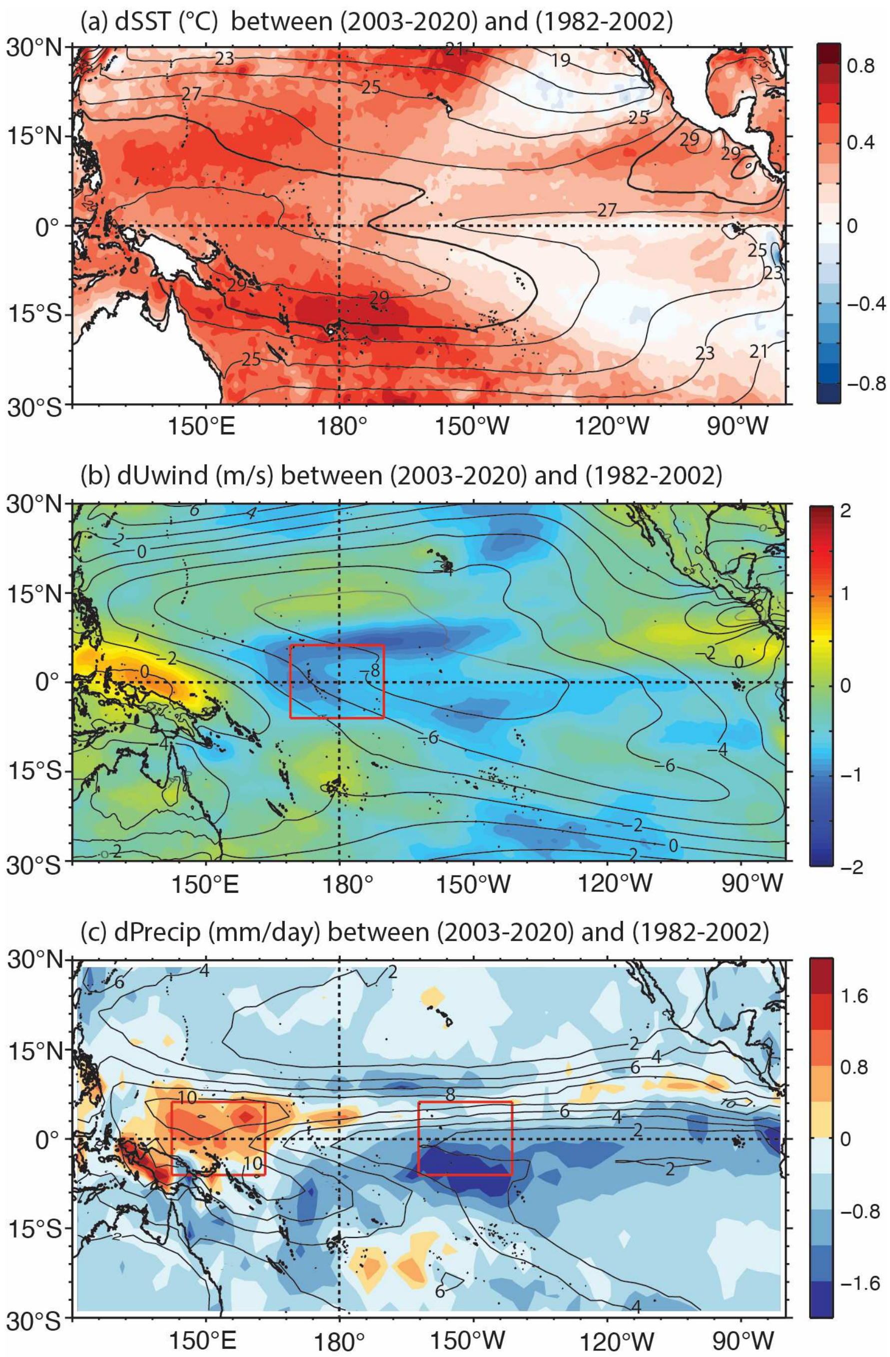

Figure 7. Epoch difference map of the February−July mean (a) SST from OISSTv2, (b) zonal wind at 850 hPa from ERA5, and (c) precipitation from the CMAP, obtained by subtracting the period 1982−2002 from the period 2003−2020. The epochal differences in the zonal wind and zonal precipitation gradient are estimated over the regions in the red boxes in (b) and (c), respectively.

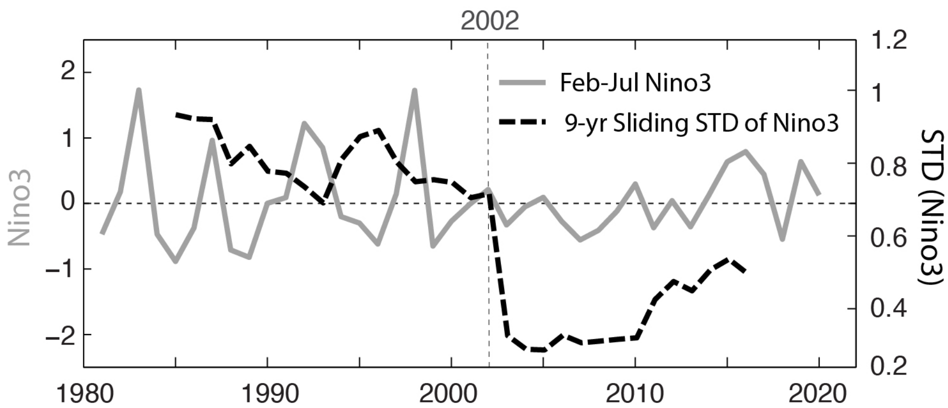

Figure 8. February to July mean Nino3 time series (solid gray line) and its nine-year running standard deviation (dashed black line).

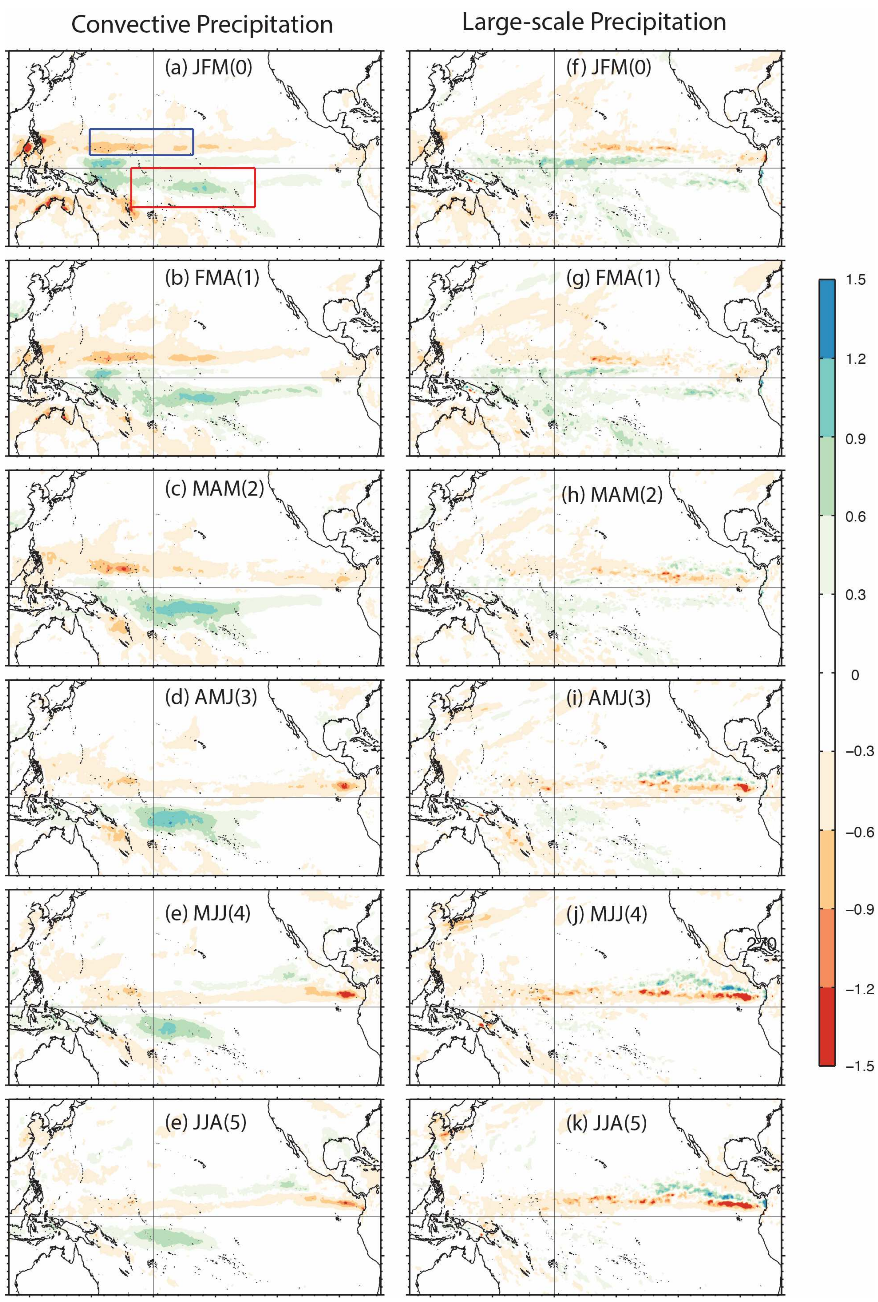

Figure 9. Lagged linear regression of the (left) convective (right) large-scale components of the precipitation on the JFM mean SST anomalies over the SEP region for the post-2003 period. The boxes in (a) indicate the domains for the precipitation index in Figure 10.

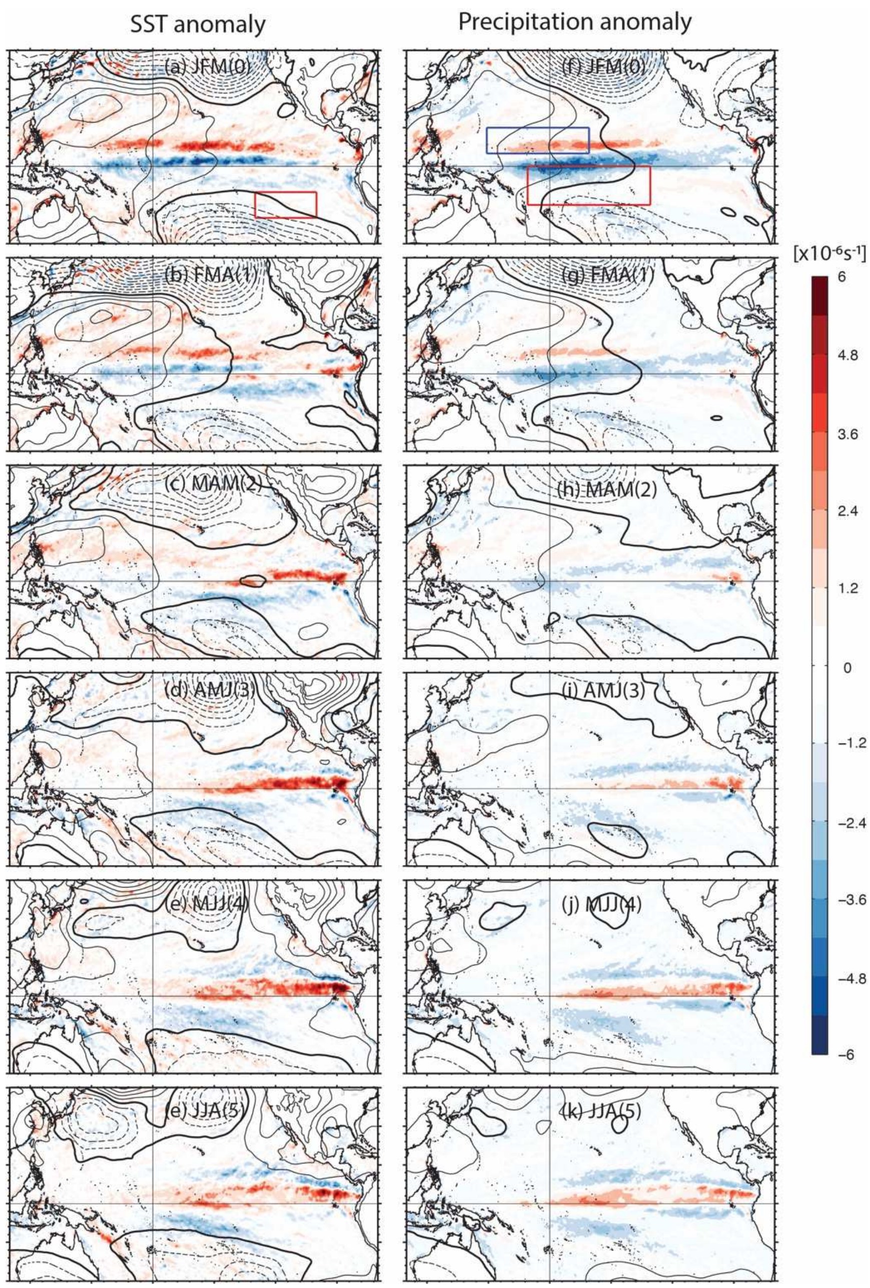

Figure 10. Lagged linear regression of the divergence of 1000 hPa winds (shading: unit s^{-1}) and geopotential height anomalies at 850 hPa (contour) on the JFM mean (left) SEP index and (right) precipitation index for the post-2003 period. The SEP index is estimated for the mean SST over the red box domain in (a), and the precipitation index for the mean convective precipitation difference between the red and the blue boxes in (f). The contour interval for the geopotential height anomalies is 6 m, the negative contours are dashed, and the zero contour is the thick line.

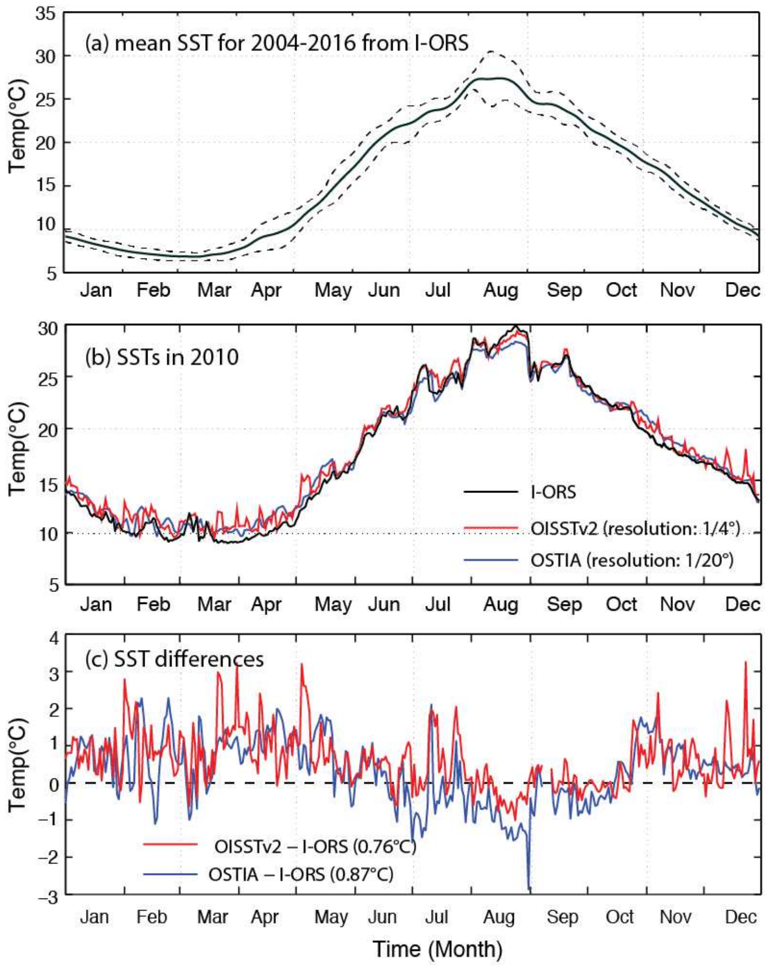

Figure S1. Time series of the surface temperature at the center of the Yellow and East China Seas. (a) Mean surface temperature (solid line) with ± one standard deviation (dashed lines) observed at a depth of 3 m from the Ieodo Ocean Research Station (I-ORS; see Figure 1a for the location; Ha et al. 2019) for the period 2004−2016. (b) Observed surface temperature in 2010 from the I-ORS (black) and SSTs from the gridded datasets, i.e., OISSTv2 (red) and OSTIA (blue), and (c) the differences between the gridded datasets and the in-situ observation. The numbers in parentheses in (c) indicate the standard deviation between the SSTs from the gridded data and the observed surface layer temperature from the I-ORS in 2010, respectively. This comparison shows that both datasets are congruent with the in-situ observations (r > 0.99; Figure S1), while the standard deviation for OISSTv2 from the observation (0.76°C) is somewhat lower than for the OSTIA (0.87°C). The OSTIA dataset has had a higher horizontal resolution of 1/20° but a much shorter data span since 2006 than OISSTv2.

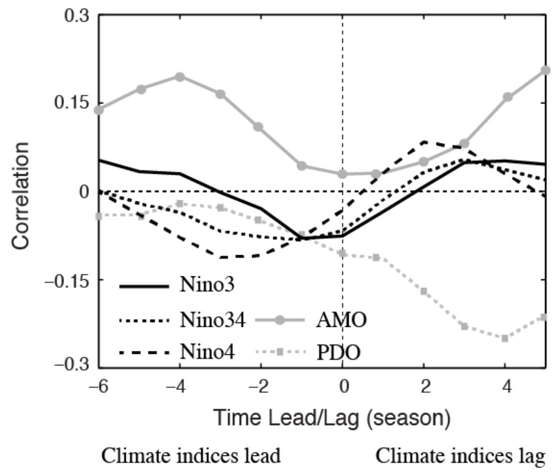

Figure S2. Cross correlations of the YECS summer SST index with climate indices (i.e., Nino3, Nino34, Nino4, AMO, PDO) at seasonal leads/lags for the period 1982−2020. Every correlation is not significant at the 95% confidence level.